Nucleation of bcc Iron in Ultrathin fcc Films

Albert Biedermann, Michael Schmid, and Peter Varga
Institut für Allgemeine Physik, Vienna University of Technology, A-1040 Vienna, Austria
(Received 13 September 2000)

Needle-shaped bcc nucleation centers in fcc films of Fe on Cu(100) are observed by scanning tunneling microscopy. They form virtually without mass transfer and nearly under conservation of volume, which causes a large strain within the nascent bcc grain. The corresponding strain energy almost equals the gain in structural energy, rendering the bcc nucleation very sensitive to any effect influencing this subtle balance. We suggest that modifying the film by straining, alloying, or surface adsorption may inhibit the bcc nucleation and lead to thick metastable fcc films.

DOI: 10.1103/PhysRevLett.86.464 PACS numbers: 68.55.–a, 64.70.–p, 75.70.–i, 81.30.–t

The epitaxial system Fe/Cu(100) has been studied extensively for the last decade owing to its ability to stabilize the fcc phase and also entirely novel ferromagnetic phases of Fe at low temperatures. Besides their relevance for various other thin film issues, these experiments aim at a better understanding of the interrelation between structure and magnetism, which is of increasing importance for the design of special purpose magnetic thin films. The prototypical phase transitions of Fe are of interest in several research areas including geophysics, metallurgy, and computational materials science. The fcc (γ) to bcc (α) phase transition, which occurs in bulk Fe at 1184 K upon quenching the solid, has been studied for a long time due to its role in steel hardening and shape memory alloys (martensitic transition). In the context of ultrathin films this phase transition attracts attention as it defines the upper limit of the stability range of (metastable) fcc films grown on fcc substrates. Previous studies showed that the critical thickness for the transformation of the fcc Fe film to the bcc structure depends on the presence of surfactants [1,2], temperature [3,4], and strain [5]. Coadsorption of carbon and oxygen containing molecules showed the most spectacular effect by delaying the phase transition by up to ~60 monolayer (ML) or 6 times its normal stability limit [1]. However, while the morphology of the larger bcc grains is now relatively well known [5–9], a model of the actual nucleation process, which could explain the large variation of the critical thickness, is still missing.

In this Letter, we present a direct view of a very early stage of the bcc nucleation on an atomic scale. Knowledge of the precise atomic structure of the nucleation centers enables us to study in detail the determining factors of the initial stages of the phase transition. Our STM images reveal the nucleation centers as nanometer-sized bcc crystals, which form free of dislocations and are therefore exposed to a very high strain. The corresponding strain energy balances the gain in structural energy, which leads to the hypothesis that any effect, which can shift this subtle balance provides control over the nucleation process.

The deposition of the Fe films was done in ultrahigh vacuum by evaporation from the tips of Fe wires heated by electron bombardment. The deposition rate of 0.5–1 ML/min was measured using a quartz microbalance and was held constant by flux control. Additionally, the layer thickness was independently estimated by quantitative Auger electron spectroscopy (AES). The STM was operated using an electrochemically etched W tip. Both deposition and imaging were done at 300 K.

Within the thickness range of 5–10 ML, room temperature films are fcc with an estimated tensile strain of ~1% [5,10]. Probing the surface after deposition of 7 ± 1 ML Fe we find a rather flat surface with the exception of small islands. We also see the previously observed "needle" structures [5,7–9], i.e., weakly protruding stripes, which have been related to misfit dislocations [5,7,9,10] in analogy to a wide range of stress relaxation phenomena in ultrathin films. We will demonstrate, however, that this is not the case for this system. Three typical occurrences are marked with arrows in the overview topography displayed in Fig. 1A. While the length of these stripes varies, their width of 2 nm is remarkably uniform. The atomically resolved image of the needle surface shown in Fig. 1B reveals its bcc(110) surface structure. The atom rows are tilted by 15°, but still fit seamlessly to the fcc lattice on both sides. This setup is similar to the Pitsch orientational relationship between larger bcc fibers and the fcc host lattice found by electron microscopy in ~100 ML films [6] and by scanning tunneling microscopy in 10–20 ML films [8,9]. There are, however, important differences: Comparing the atomic geometry of the discussed "initial" bcc structure with that of the ideal bcc structure of larger grains reveals immediately the large strain within the observed needles (Fig. 2). The strongest strain component is a tensile strain, $\varepsilon_y \sim 9\%$, perpendicular to the needle axis due to the commensurable nature of the needles (cf. equidistant lines in Fig. 1B). Apparently, the resulting in-plane shear strain reduces the tilt angle of the atom rows from its ideal value, $\alpha \sim 19.5°$, to the measured 15°. This is important information since it shows that the structure is in fact a transition structure, significantly different from the relaxed bcc fibers [6] observed in the thicker films.

What is the structure of the needles in the vertical dimension? The significant bulging of the needles and the observation of needles crossing monatomic step edges points

 0031-9007/01/86(3)/464(4)$15.00

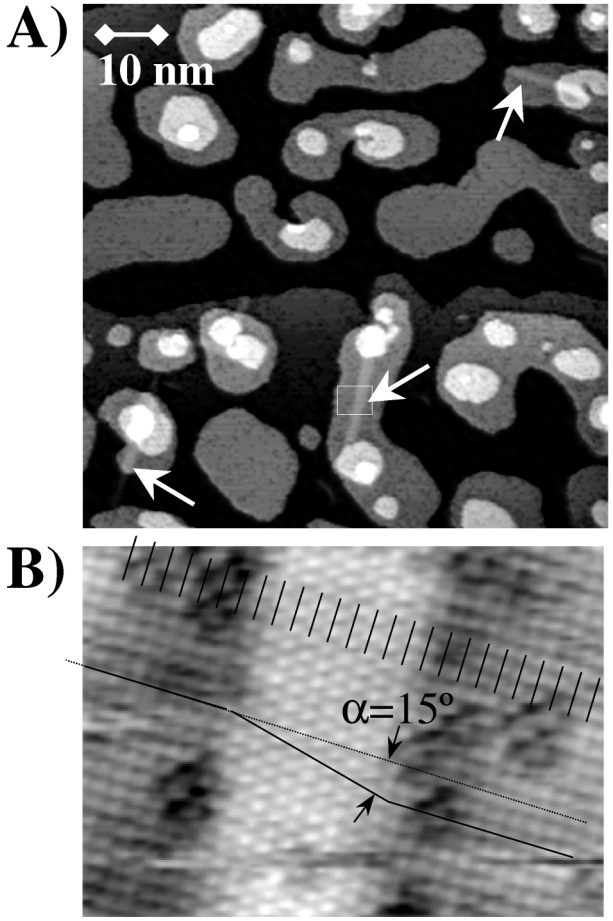

FIG. 1. (A) STM topography after deposition of 7 ± 1 ML Fe on Cu(100). Slightly elevated (brighter) stripes or "needles" are marked (arrows). They appear to nucleate mainly at small 3D islands. (B) Atomically resolved surface of one of the needles (area marked by white rectangle in overview topography). The equidistant lines indicate the nearly equal spacing of atom rows across the needle and the surrounding fcc lattice. Sample voltage/current − 1 V/10 nA (A) and −3 mV/10 nA (B).

to a multilayer structure. This conjecture is supported by the shape of the cross sections through the needle surface: First of all, near the center of the needle where the bcc lattice matches the fcc lattice underneath (cf. Fig. 2A), a very thin bcc needle (mono- or bilayer) should show a minimum in apparent height, which is not the case. Further, needles crossing step edges and islands may be utilized to determine the needle thickness in a more quantitative way: Fig. 3 shows a needle crossing a single- and a double-layer island with all levels equalized. The needle elevation is largest on the topmost level III and lowest on level I, the completed monolayer. The elevation difference between adjacent levels of 0.01–0.03 nm (Fig. 3C) is close to the expected difference between the interlayer distances of fcc(100) iron (~0.180 nm) and bcc(110) iron (0.203 nm). The linear elastic calculation, described in the next paragraph, predicts a significant vertical cross contraction ε_z due to the high in-plane strain ε_y which reduces the thickness difference per layer to half of its value: $b \sim 0.01$ nm.

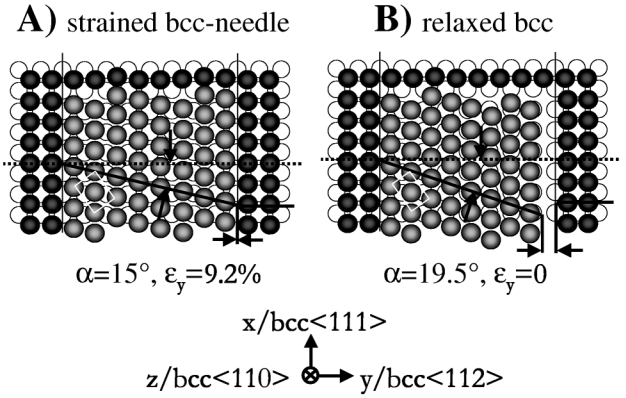

FIG. 2. Schematic model of the film-substrate relation for (A) the observed strained and (B) a relaxed bcc needle. A strain of $\varepsilon_y \sim 9\%$ is necessary to close the gap between the relaxed bcc needle and the surrounding fcc lattice. The white rectangle marks a bcc(110) unit cell.

This is in agreement with the difference of the cross sections through levels I and II (cf. Fig. 3C). Extrapolating the needle elevation to zero allows a crude estimate of the local thickness of the needles. We presume the existence of about three additional bcc layers below the topmost completed monolayer (level I). The absence of reconstruction near the interface can be explained by strong intermixing with Cu [11]. The section of the needle crossing the very

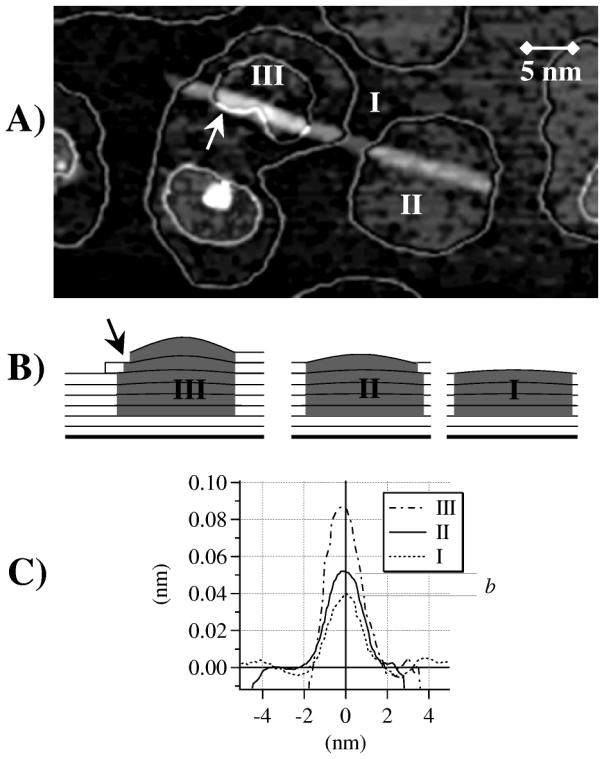

FIG. 3. Needle crossing single- and double-layer islands. (A) Leveled STM topography; the needle brightness correlates with the local number of bcc-Fe layers. (B) Schematic cross sections. (C) Measured cross sections of the needle. The topmost needle layer in the small level III area is laterally relaxed (arrows) since the needle is very close to the island edge.

small topmost island level III shows a very high elevation difference of 0.03 nm with respect to the island level II. This indicates a significant lateral strain relief and an almost complete absence of cross contraction for the topmost layers in this small area, which can be easily explained by the immediate proximity of needle and island edge.

Why are the needles formed? In thin films, the phase transition typically occurs if the structural energy gain outweighs the energy necessary to generate the mismatch between film and substrate. While this is certainly correct for the relaxed bcc film, the situation is different for the discussed nucleation process. Here, the relatively weak mismatch with the substrate, discussed in more detail below, is less important than the large strain that is built up within the needle. To show this we use linear elasticity theory to estimate the strain relations and the strain energy. At first we assume a rigid surrounding fcc lattice, which dictates both a strain parallel to the needle axis, $\varepsilon_x = 2.95\%$, and a perpendicular strain, $\varepsilon_y = 9.2\%$ (cf. Fig. 2). In order to model the center of the needles, the bcc grain is allowed to relax freely in the vertical direction, whereas for the edges the bcc structure is vertically pinned to the fcc lattice (full shape and volume conservation). The resulting in-plane shear strain ε_{xy}, assuming a rigid fcc lattice, causes a decrease of the angle α from 19.5% for an undistorted bcc lattice to 14.1° (15.6°) for the edge (center) of the needle, which agrees very well with the measured angle of 15°. For the purpose of comparison with other fcc-to-bcc pathways, a novel "needle path" (cf. top row Fig. 4B) may be constructed by linking the observed strain deformation of the bcc lattice to a shear deformation of the fcc lattice. In Fig. 4A, the strain energy per atom corresponding to this "needle path" is plotted in dependence of the ratio of the lattice constants c and a, which is usually used to parametrize the distortion.

Thermodynamic experimental data suggest that the bcc lattice is favored with respect to the fcc lattice by 50–60 meV/atom (cf. [12,16], and references therein). Therefore, it is obvious that the calculated energy of the fully strained needle would be too high to allow the needle formation. However, it should be noted that the linear elastic calculation very likely overestimates the strain energy for larger tensile distortions, because the lattice typically becomes softer for increasing interatomic distances, which is clearly the case. Second, the surrounding fcc lattice cannot be infinitely stiff and the needle will relax at least a little. A thorough analysis of the STM image suggests that the needles in our films relax less than ~2% with respect to their immediate fcc environment (cf. Fig. 1A). A stress relief of only 1%–2%, however, already decreases the strain energy by 20–30 meV/atom. This may explain also why the needles initially do not grow beyond a width of 8 atom rows: The near surface region of the needle will be able to relax slightly more depending on its height to width aspect ratio: The smaller the needle width, the larger the energy gain due to the additional relaxation. In conclusion, the actual strain energy within the needle

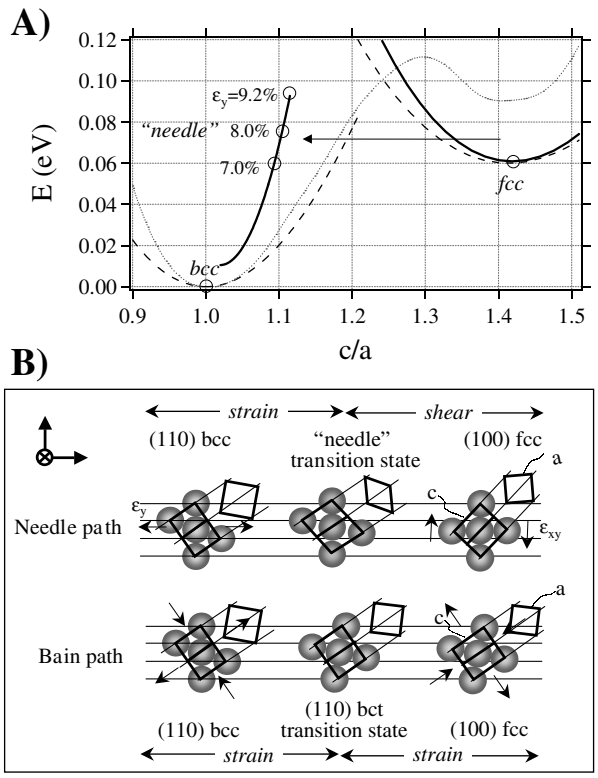

FIG. 4. (A) Linear elastic approximation of the total energy along the experimentally observed "needle path" approaching the needle structure from the fcc side by shear and from the bcc side by strain in dependence of the lattice constant ratio c/a (full line). The fcc side is offset by experimental values for the energy difference between the (bulk) bcc and fcc structures (Ref. [12]). An additional small tensile strain $\varepsilon_x = 2.95\%$ (1.0%) is assumed for the bcc (fcc) side. Also shown is a first-principles result for the Bain path by Moroni *et al.* (dotted line, Ref. [13]) and its linear elastic approximations (dashed line). Elastic constants for bcc and fcc Fe taken from Refs. [14] and [15]. (B) Schematic model of the distortions and applied strains for both pathways.

and its near environment will be very similar to or only slightly smaller than the gain in structural energy.

What is the role of the mismatch energy in the energy balance? The width of the needles in our film is a small multiple of the structure's "magic number" $\tan^{-1}(\alpha) \sim 4$: mostly 8 atom rows. This enables simultaneously a perfect matching with the fcc lattice at both sides and a shear-stress relaxed structure. Also, the strained bcc structure is still commensurable at the substrate interface in the direction perpendicular to the needle axis, which minimizes the mismatch energy. Assuming a sharp transition from bcc to fcc at the interface leads to an estimated mismatch energy of the order of 0.1 eV per interface atom or 20 meV/atom for a 5 layer film based on estimates of the bridge site energy of an Fe adatom on Fe(100) [17]. However, the fcc-bcc interface might reconstruct to some degree in order to minimize the mismatch energy even further by smoothing the structural transition between fcc and bcc near the interface.

Since the small mismatch energy is balanced by an equally small sum of the rather large strain energy loss

and structural energy gain, even a small change of either strain or structural energy strongly influences the critical thickness of the bcc nucleation. The preparation of films with higher tensile strain or alloying the film with fcc stabilizers, e.g., C or Ni, can shift the energy balance and prevent the bcc nucleation. Indeed, the observation of fcc films growing up to a thickness 6 times its normal stability limit in the presence of the surfactants C and O was explained by C incorporation [1]. A preference of C or O for adsorbing in an fcc(100) rather than bcc(110) hollow site may be an alternate or additional explanation for this phenomenon. Also, the recent suggestion of an early nucleation of the bcc structure in Fe/Ni(100) films [5] can be now motivated by the weak (1%) "transition-promoting" (because strain reducing) compressive strain in these films, in contrast to the "transition-hindering" tensile strain in the Fe/Cu(100) system.

Are the needles indeed a necessary transition state for the fcc-bcc transition? The process suggested by Pitsch [6] is relatively similar to the process observed by us, but assumes a relaxed bcc grain as nucleation center, which includes mass transfer to fill the gap visible in the schematic representation in Fig. 2B. However, the needle has to nucleate with a certain minimum size to overcome the mismatch at its ends. Spontaneous finite size nucleation, i.e., nondiffusive in the language of metallurgy, is not possible if mass transfer is involved. The process observed by us, however, is clear evidence that a mass-transfer-free nucleation is possible. The pathway starts with a spontaneous shear deformation, which should be imagined as small (less than half the next neighbor distance) individual shifts of the atom rows parallel to the needle axis (cf. Fig. 2). This pathway avoids mass transfer at the needle ends and guarantees a minimum transition barrier, since no atom crosses a bridge site. Both conditions, negligible mass transfer and low barrier, are necessary to explain the spontaneous needle formation at 300 K. Subsequently, the needle can contract perpendicularly accompanied by inclusion of atoms one by one into the zipperlike opening gap between relaxed needle and fcc lattice (cf. Fig. 2B).

In summary, we have studied the nucleation centers of the bcc structure in ultrathin fcc iron films deposited at room temperature on Cu(100). They are revealed as narrow, elongated bcc crystals (needles), which are commensurable with the fcc lattice and therefore substantially strained. The corresponding strain energy almost balances the gain in structural energy. Every measure influencing either the strain or the structural energies should permit sensitive control over the nucleation process and the critical film thickness. The needles can form without mass transport and with a minimum barrier, which explains the spontaneous nucleation at 300 K.

We gratefully acknowledge support by the "Fonds zur Förderung der Wissenschaftlichen Forschung" (Austrian Science Foundation).

[1] A. Kirilyuk, J. Giergiel, J. Shen, M. Straub, and J. Kirschner, Phys. Rev. B **54**, 1050 (1996).
[2] J. Thomassen, F. May, B. Feldmann, M. Wuttig, and H. Ibach, Phys. Rev. Lett. **69**, 3831 (1992).
[3] S. Müller, P. Bayer, C. Reischl, K. Heinz, B. Feldmann, H. Zillgen, and M. Wuttig, Phys. Rev. Lett. **74**, 765 (1995).
[4] K. Heinz, S. Müller, and P. Bayer, Surf. Sci. **352–354**, 942 (1996).
[5] J. Shen, C. Schmidthals, J. Woltersdorf, and J. Kirschner, Surf. Sci. **407**, 90 (1998).
[6] W. Pitsch, Philos. Mag. **4**, 577 (1959).
[7] J. Giergiel, J. Shen, J. Woltersdorf, A. Kirilyuk, and J. Kirschner, Phys. Rev. B **52**, 8528 (1995).
[8] K. Kalki, D. D. Chambliss, K. E. Johnson, R. J. Wilson, and S. Chiang, Phys. Rev. B **48**, 18 344 (1993).
[9] M. Wuttig, B. Feldmann, J. Thomassen, F. May, H. Zillgen, A. Brodde, H. Hannemann, and H. Neddermeyer, Surf. Sci. **291**, 14 (1993).
[10] A. Schatz and W. Keune, Surf. Sci. **440**, L841 (1999).
[11] T. Detzel and N. Memmel, Phys. Rev. B **49**, 5599 (1994).
[12] G. L. Krasko and G. B. Olson, Phys. Rev. B **40**, 11 536 (1989).
[13] E. G. Moroni, G. Kresse, J. Hafner, and J. Furthmüller, Phys. Rev. B **56**, 15 629 (1997).
[14] H. D. Ledbetter, Phys. Status Solidi A **85**, 89 (1984).
[15] *CRC Handbook of Chemistry and Physics,* edited by D. R. Lide and H. P. R. Frederikse (CRC Press, Boca Raton, 1997), 78th ed.
[16] C. Zener, in *Phase Stability in Metals and Alloys,* edited by P. S. Rudman (McGraw-Hill, New York, 1967), p. 25.
[17] M. T. Kief and W. F. Egelhoff, Phys. Rev. B **47**, 10 785 (1993).